Noncollinear magnetic configurations and substrate-mediated interactions in Mn trimers on the GaN (000$\bar{1}$) surface

Diego Hunt,[1,*] María Andrea Barral,[1] Arthur R. Smith,[2] and Valeria Ferrari[1]

[1]*Instituto de Nanociencia y Nanotecnología, CNEA-CONICET, Departamento de Física de la Materia Condensada, GIyA, CAC-CNEA, 1650 San Martín, Buenos Aires, Argentina*

[2]*Nanoscale and Quantum Phenomena Institute, Department of Physics and Astronomy, Ohio University, Athens, Ohio 45701, USA*

(Received 12 September 2020; revised 5 February 2021; accepted 15 February 2021; published 12 March 2021)

Collinear and noncollinear calculations based on density functional theory are carried out to elucidate the magnetic ordering of Mn trimers on a GaN (000$\bar{1}$) substrate. These trimers had previously been observed in $3a \times 3a$ surface reconstructions through Mn deposition onto the N-polar face of wurtzite GaN(000$\bar{1}$). We start off by studying the effect of spin orbit coupling for the case of monomers and dimers of Mn atoms on top of a GaN surface. Based on an effective spin Hamiltonian, we estimate the magnetic anisotropy energy (MAE) for those cases and found that it is four orders of magnitude weaker than the exchange magnetic coupling between Mn adatoms. In the Mn trimer case, the magnetic ground state has the Mn spins in-plane with the GaN surface in which the relative spin orientation within each trimer is noncollinear due to the competition between the two antiferromagnetic interactions that affect each Mn spin in the trimer, which leads to the found energy minimum with 120 degree angles between the spins. By exploring the nature and fundamental mechanisms for the magnetic interaction among the Mn trimers, we find that the surface states of the substrate play a key role, involving a Ruderman-Kittel-Kasuya-Yosida (RKKY)-type interaction. We report on an electron-mediated long-distance exchange coupling between localized magnetic moments on a GaN(000$\bar{1}$) surface.

DOI: 10.1103/PhysRevB.103.094418

I. INTRODUCTION

Frustrated magnets in 2D systems have recently attracted major scientific interest as they can manifest diverse exotic magnetic states, such as spin ice and quantum spin liquids which in turn play a key role in high-temperature superconductors [1,2]. Their complex magnetic properties are usually related to the competition of different physical interactions. On one hand, we have the symmetric or Heisenberg exchange interaction between spin centers which modulates the alignment of the magnetic moments. On the other hand, we have the antisymmetric exchange or Dzyaloshinskii-Moriya (DM) interaction, whose nature stems from the spin-orbit coupled electrons, and it is crucial in the formation of magnetic skyrmions and in the stabilization of noncollinear metallic magnets [3,4]. Further, spin-orbit coupling (SOC) leads to the magnetic anisotropy energy (MAE), assessing an energy barrier for the easy and hard axis orientation of the magnetic moments.

An ideal system to study the phenomenon of frustration in magnetism is the adatoms or small metallic clusters on top of surfaces. The interest in frustrated magnetic nanostructures over nonmagnetic or ferromagnetic surfaces have risen due to their potential applications in spintronics [5]. In particular, antiferromagnetic nanostructures have attracted lots of attention in recent years [6–8] as they provide more stability for data retention against magnetic field perturbations, compared to ferromagnetic materials. In addition, these antiferromagnetic materials present much faster spin dynamics, thus paving the way towards ultrafast data processing [9].

Concerning the study of Mn clusters on magnetic and nonmagnetic substrates, several studies based on electronic structure calculations have been reported. Bergman *et al.* focused on noncollinear magnetic interactions in Cr and Mn clusters deposited on Cu(111) substrates [10,11]. They found that Cr clusters prefer collinear spin configurations while Mn clusters might exhibit noncollinear configurations even for clusters that are not frustrated from a geometric viewpoint. Cardias *et al.* [12] reported the electronic and magnetic structure of Mn nanowires adsorbed on Ag(111) and Au(111) surfaces. They found that the noncollinear magnetic ordering of Mn nanostructures on Ag(111) is due to strong exchange interactions between the metal ions but in the case of Au(111), DM interactions lead to complex magnetic structures of the clusters. Noncollinear antiferromagnetic behavior, of both dimers and trimers of Mn atoms on Ni(001) surfaces, was also reported by Lounis *et al.* [13] in which the magnetic nature of the substrate plays an active role in the modulations of the magnetic properties of the nanoclusters. Therefore, understanding the magnetic properties of small metallic clusters on different substrates includes not only determining the spin orientation of the individual metal centers but also studying the influence of the substrate on the underlying mechanisms governing the magnetic interactions among them. One of the challenges in both physics and materials science is to obtain long-range magnetic order in low-dimensional materials. In this context, single magnetic adatoms and small magnetic

*hunt@tandar.cnea.gov.ar

clusters adsorbed on substrates are very promising building blocks for spin processing information and spintronics [14]. There are basically two interactions that represent the main mechanisms among spins on metallic surfaces, namely the dipolar interaction and the conduction electron-mediated Ruderman-Kittel-Kasuya-Yosida (RKKY) interaction. While direct Heisenberg exchange cannot properly describe the indirect coupling among spins on metallic surfaces, the RKKY interaction has successfully explained the typical oscillatory behavior observed, that is, an alternation of the coupling interaction being either ferromagnetic or antiferromagnetic as a function of the distance between spins [15–17].

In our previous paper [18], Mn atoms were deposited onto the N-polar face of wurtzite gallium nitride GaN(000$\bar{1}$) and, depending on the deposition temperature, two surface reconstructions were obtained. At low temperatures, a metastable $3a \times 3a$ structure forms, which upon mild annealing converts to a more stable $\sqrt{3}a \times \sqrt{3}a$ structure through an irreversible phase transition. Using *ab initio* techniques, we explored the energetics of this system proposing models in agreement with scanning tunneling microscopy (STM) images as well as reflection high energy electron diffraction (RHEED) data. We found that the lowest energy model for the $3a \times 3a$ structure was composed of trimers of Mn adatoms, while the most stable model for the $\sqrt{3}a \times \sqrt{3}a$ structure involved Mn atoms substituting for surface Ga atoms. Recently, we found that this $\sqrt{3}a \times \sqrt{3}a$ structure corresponds to a MnGaN-2D surface alloy with high spin polarization and room temperature ferromagnetism [19].

In the present work, we study the magnetic properties of the $3a \times 3a$ observed surface reconstruction composed by Mn trimers using density functional theory (DFT) calculations. This paper is organized as follows. In Sec. II we briefly describe the electronic and structural properties of the N-polar surface of gallium nitride [GaN(000$\bar{1}$)]. In Sec. III A we analyze the magnetic properties of one and two Mn adatoms on a GaN(000$\bar{1}$) substrate and estimate the different magnetic contributions to the total energy using an effective spin Hamiltonian. In Sec. III B we describe the main structural features of the observed $3a \times 3a$ surface reconstruction of GaN(000$\bar{1}$) composed of Mn trimers, and we focus on the magnetically frustrated Mn trimers and the effects of noncollinear magnetism. Finally, in Sec. III C, we find that the substrate plays an essential role on the magnetic interactions among the Mn trimers. We propose a Ruderman-Kittel-Kasuya-Yosida (RKKY) interaction mechanism to explain the nature and magnitude of the exchange interactions among Mn clusters on the GaN(000$\bar{1}$) surface.

II. PHYSICAL PROPERTIES OF THE GaN(000$\bar{1}$) SURFACE

Before proceeding to the main results of the present paper, it is useful to briefly describe the electronic properties of the GaN(000$\bar{1}$) surface compared to bulk GaN. Experimentally, several GaN(000$\bar{1}$) reconstructions have been obtained, such as 1×1, 3×3, 6×6, and $c(6 \times 12)$ [20]. In this work, we are interested in the 1×1 structure which consists of a single monolayer of Ga atoms, bonded in top sites above N atoms of a N-terminated GaN bilayer. The bond length between the surface Ga atoms and the N atoms in the first subsurface layer

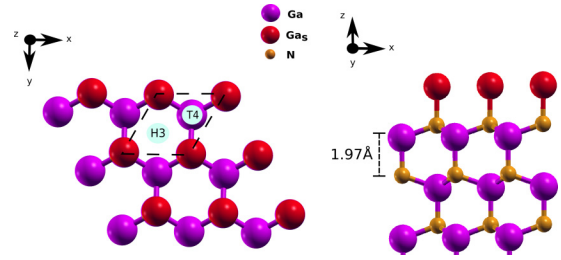

FIG. 1. Structural representations of the GaN(000$\bar{1}$) 1×1 surface. The color coding for the different atoms is stated in the legend where Ga$_s$ stands for the Ga atoms at the surface. Left panel: Top view with the two high-symmetry sites marked H3 and T4. Right panel: Side view of the structure stating the distance between Ga and N monolayers.

is equal to 1.97 Å (in GaN bulk structure, the Ga-N distance is 1.94 Å). There are two different high-symmetry points on the clean GaN(000$\bar{1}$) surface, H3 and T4 as shown in Fig. 1. Both positions correspond to a hollow site formed by the triangle composed of three surface Ga atoms (Ga$_s$); for T4, it is above the second layer Ga, whereas for H3, it is above the hollow site of the first GaN bilayer.

It is well known, both from the experimental and theoretical viewpoints, that the GaN bulk structure has an insulator behavior [21] ($E_{gap} \sim 3.35$ eV) in which the major contribution to the valence band maximum corresponds to the N p orbitals [21,22]. The electronic properties of the GaN(000$\bar{1}$) surface are significantly different compared to the bulk ones, being characterized by a metallic behavior through their surface states. Those GaN surface states are noticeable in the band structure of the bare GaN(000$\bar{1}$) 1×1 surface shown in Fig. 2. The electronic structure displays features of metallic-like behavior with levels crossing the Fermi level, with the Ga$_s$ atomic orbitals being the major contribution to the electronic states in the vicinity of the Fermi level.

A detailed inspection of the GaN(000$\bar{1}$) 1×1 surface electronic structure shows the presence of three bands, hereafter labeled as B1, B2, and B3, corresponding to GaN surface states appearing within the bulk band gap [23–26]. The B1

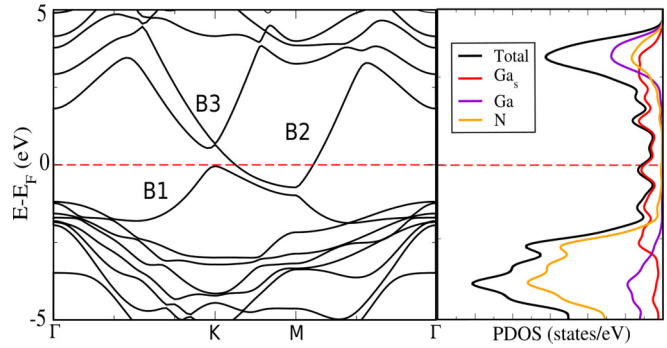

FIG. 2. Band structure (left) and projected density of states (PDOS) (right) for the bare GaN(000$\bar{1}$) 1×1 surface along $\Gamma \rightarrow K \rightarrow M \rightarrow \Gamma$ points. The Fermi level is marked by a red dashed line. The PDOS is projected onto the different atoms of the structure. The major contribution of the electronic states close to the Fermi level corresponds to the Ga$_s$ atomic levels.

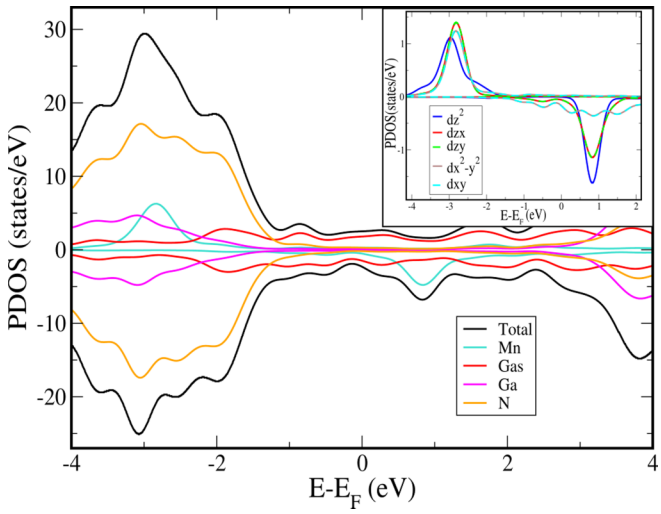

FIG. 3. Total density of states and projected density of states (PDOS) for one Mn adatom on a GaN(000$\bar{1}$) substrate. The positive (negative) DOS and PDOS represent majority (minority) states. The major contribution of the electronic states close to the Fermi level corresponds to the Ga$_s$ atomic levels. The double degeneracy of the Mn d orbitals is shown in the inset.

band is completely occupied, the B3 one is completely unoccupied, and B2 is a partially filled band. Both B3 and B2 bands present a parabolic free-electron-like band behavior, whose dispersion relations are centered around the K and M points, respectively. In particular, the asymmetry of the B2 band with respect to the M point suggests an anisotropic behavior of this surface state.

III. RESULTS

A. Monomers and dimers of Mn atoms on the GaN(000$\bar{1}$) substrate

As a first step towards understanding the magnetic properties of Mn trimers on the GaN(000$\bar{1}$) substrate, we evaluate the electronic structure of one and two Mn adatoms by means of noncollinear calculations including spin-orbit coupling. Details of the DFT calculations and the unit cells used are described in Appendix A. We first place a Mn adatom on the H3 adsorption site in the $3a \times 3a$ GaN(000$\bar{1}$) unit cell, given that H3 is the most stable adsorption site on the surface [18]. After performing atomic relaxation, the distances from the Mn atom to each of its nearest-neighbor surface Ga$_s$ atoms (i.e., the Mn-Ga$_s$ distances) are all equivalent and equal to 2.52 Å. The Mn magnetic moment is 4.36 μ_B (with the total magnetic moment of the cell being 4.52 μ_B). Figure 3 depicts the total density of states (DOS) and the projected density of states (PDOS) of the Mn monomer on the GaN(000$\bar{1}$) substrate. It is clearly seen that the Mn $3d$ majority spin states are all below the Fermi level and the minority states are all above it, which implies a spin $S = 5/2$ configuration. Interestingly, for the Mn adatom, a detailed examination of the electronic states shows that Mn d orbitals split into three energy levels, two of which are doubly degenerate, consistent with the C_{3v} symmetry of the Mn site [27]. Concerning how the electronic properties of the GaN(000$\bar{1}$) are modified by the presence of one Mn adatom, an inspection of the PDOS shows that the major contribution of the electronic states close to the Fermi level corresponds to the Ga$_s$ atoms through their surface states.

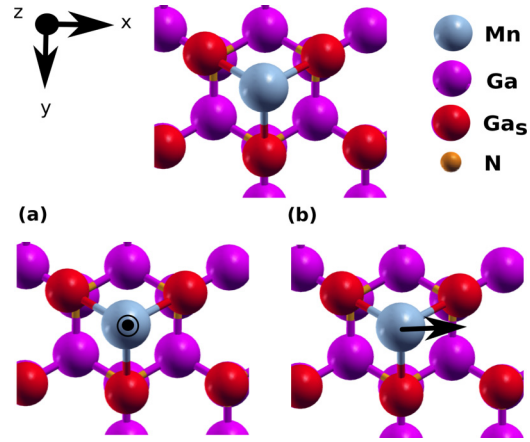

FIG. 4. Structural model of the relaxed structures for the monomer case, a Mn adatom at an H3 site on top of the GaN(000$\bar{1}$) surface. Top panel displays the top view of the structure while the bottom panels indicate the magnetic spin orientations of the Mn adatom with respect to the GaN substrate (top view). (a) out-of-plane; (b) in-plane spin configurations.

To evaluate the magnetic anisotropy energy (MAE) for the monomer, an effective spin Hamiltonian describing the magnetic properties of a metallic adatom on a given surface can be expressed as

$$H_{\mathrm{MAE}} = KS_z^2 + E\left(S_x^2 - S_y^2\right), \tag{1}$$

where K is the axial magnetic anisotropy constant, E is the transverse magnetic anisotropy parameter, and S_i stands for the i component of the total spin $\mathbf{S}$ for the Mn adatom. K and E can be estimated through the corresponding total energies considering the magnetization axis along each of the three nonequivalent directions, one of them perpendicular to the GaN(000$\bar{1}$) surface and the other two in-plane with the substrate. For the case of one Mn adatom on the GaN(000$\bar{1}$) surface, we found that the total energy for both in-plane spin orientations (namely, x axis and y axis) are equal. Hence, our calculations show that the transverse magnetic anisotropy constant E is zero. This result is consistent with the C_{3v} symmetry of the Mn site. Therefore, evaluating the total energy difference between in-plane and out-of-plane spin configurations (see Fig. 4) we can estimate K. Negative K values denote an out-of-plane anisotropy while positive values imply an in-plane anisotropy orthogonal to the z axis. In this system, K is found to have a very small negative value, more precisely $K \sim -0.5\ 10^{-3}$ meV/Mn. This value suggests that the MAE is weak for the monomer, which is consistent with the half-filled $3d$ band of the Mn atom [28].

The next step is to consider two Mn adatoms in a dimeric arrangement as shown in Fig. 5. The Mn adatoms are placed in two H3 adjacent sites on the $3a \times 3a$ GaN(000$\bar{1}$) unit cell at the initial distance of 3.19 Å, and then the structure is allowed to relax. We first evaluate the energy difference between the antiferromagnetic (AF) and the ferromagnetic (FM) configurations without considering the relative orientation of the

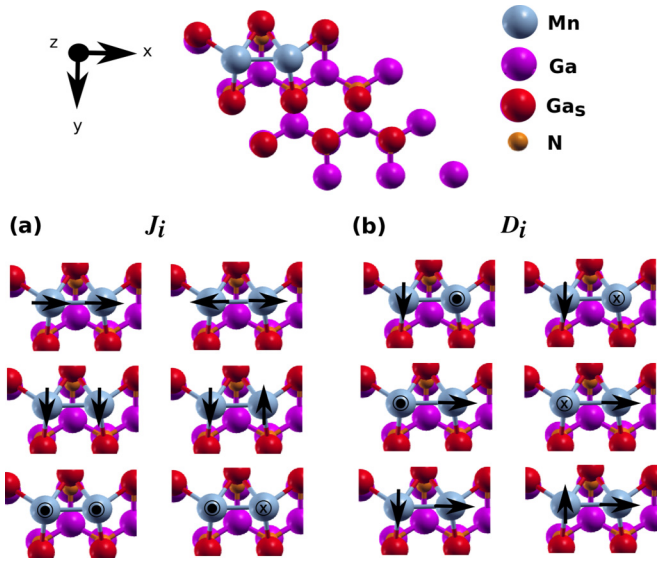

FIG. 5. Relaxed model structure for two Mn adatoms on top of the GaN(000$\bar{1}$) surface. Top panel displays the top view of the structure and bottom panel presents the magnetic configurations employed to estimate the main magnetic interaction parameters, (a) J_i, (b) D_i.

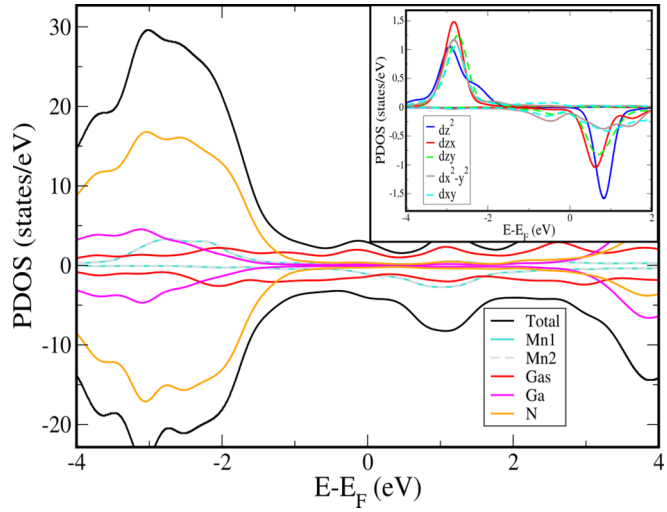

FIG. 6. Total density of states and projected density of states (PDOS) for two Mn adatoms on the GaN(000$\bar{1}$) substrate. The major contribution of the electronic states close to the Fermi level corresponds to the Ga$_s$ atomic levels. The lift of the double degeneracy of the Mn d orbitals is shown in the inset.

magnetic moments with respect to the crystal axes. Table I displays the relevant parameters after performing atomic relaxation. Namely, the Mn-Mn distance ($d_{\text{Mn-Mn}}$), the magnetic moments of Mn adatoms (μ_{Mn}), and the relative energy per Mn atom, the difference (ΔE) between the FM and the AF configurations. A first inspection of these results shows that the AF configuration is lower in energy than the FM one by 53 meV per Mn atom. The $d_{\text{Mn-Mn}}$ values and the magnitudes of μ_{Mn} are in good agreement with previous spin-polarized DFT results for embedded Mn clusters in GaN bulk [29] and also with Mn dimers adsorbed on the (111) surfaces of Cu, Ag, and Au [30,31]. Regarding the atomic structure, our results are in line with those obtained by Cui *et al.* [29]. In that work, they found that Mn clustering causes a strong local structural distortion resulting in Mn-Mn distances contracting in comparison to Ga-Ga distances in GaN bulk. This distance shortening is indicative of a strong attractive interaction between the Mn atoms.

Figure 6 shows the total DOS and the PDOS for the dimer of Mn atoms on top of the GaN(000$\bar{1}$) slab. As in the Mn monomer case, the major contribution of the electronic states at the Fermi energy corresponds to the Ga$_s$ levels but the Mn adatom contribution becomes more significant compared to the single adatom case. The structural changes upon the Mn adatoms environment in this case, compared with the single adatom, produce the loss of the C_{3v} symmetry, which results in the rupture of the d-orbitals degeneracy for the Mn levels (see inset of Fig. 6).

TABLE I. Relative energies (ΔE), Mn magnetic moments (μ_{Mn}) and Mn-Mn distances ($d_{\text{Mn-Mn}}$), for AF and FM magnetic configurations in a dimer cluster of Mn atoms on the GaN surface, as depicted in Fig. 5.

Magnetic state	ΔE (meV/Mn)	μ_{Mn} (μ_B)	$d_{\text{Mn-Mn}}$ (Å)
AF	0	4.14	2.60
FM	53	4.27	2.82

To explore the magnetic properties of the dimer, we take the crystal structure corresponding to the AF ground state. Turning to the effective spin Hamiltonian for this dimer case, along with the magnetocrystalline anisotropy energy, two additional interactions between the Mn atoms should be incorporated, namely, the magnetic exchange coupling and the Dzyaloshinskii-Moriya interaction. Thus, the corresponding Hamiltonian takes the form,

$$H = H_{\text{MAE}} + \sum_i J_i S_{1i} S_{2i} + \mathbf{D} \cdot (\mathbf{S_1} \times \mathbf{S_2}), \qquad (2)$$

where J_i are the cartesian components of the direct exchange interactions and $\mathbf{D}$ is the DM vector. $\mathbf{S_1}(\mathbf{S_2})$ represent the spin vector of atom 1(2). S_{km} with $k = 1, 2$ and $m = x, y, z$, are the cartesian components of the spin vectors $\mathbf{S_1}$ and $\mathbf{S_2}$,

The Hamiltonian parameters can be estimated using the total energies of the different magnetic configurations by mapping them onto the model Hamiltonian. In particular, to estimate the values of J_i, we consider the magnetic configurations depicted in Fig. 5(a) with the magnetic moments either parallel (FM$_i$) or antiparallel (AF$_i$) for each of the three coordinate axes. The J_i values are calculated by $J_i = \frac{\Delta E_i}{2S_i^2}$ ($S_z = 2$), with $i = x, y, z$ being ΔE_i, the energy difference between the AF$_i$ and FM$_i$ configurations, $\Delta E_i = E_{\text{AF}_i} - E_{\text{FM}_i}$. We find the same value of $J = -3.34$ meV for every space direction, thus evidencing the isotropic nature of the exchange coupling.

Regarding the magnetocrystalline anisotropy energy, we perform collinear AF calculations, with the magnetic moments being fixed along the three crystal axes, x (along the Mn-Mn bond), y, and z. By comparing the total energies of the three calculations, we conclude that the MAE is of

the order of μeV. Given that for Mn the anisotropic effects are very weak, which demands extremely accurate numerical calculations, we neglect the MAE contribution to the effective spin Hamiltonian.

To estimate the components of the DM vector **D**, we propose different magnetic configurations as the ones depicted in Fig. 5(b). The orthogonality among the magnetic moments results in the exchange contribution to the effective Hamiltonian being zero. The components of the DM vector are calculated as $D_i = \frac{\Delta E_i}{2S^2}$, where ΔE_i is the energy difference between the two magnetic configurations associated with the DM vector component in each direction, as shown in Fig. 5(b). Interestingly, we obtain $D_x = 0$. This result is expected taking into account the Moriya rules [32] obtained from symmetry arguments: If two magnetic moments have a symmetry plane orthogonal to the line that connects them, **D** must be parallel to this plane. In our case, the **D** vector must be lying in the yz plane which is a mirror plane perpendicular to the line joining the adatoms, as can be seen in Fig. 5. Indeed, $D_x = 0$, and D_y and D_z are equal to 0.025 meV and 0.070 meV, respectively.

Summarizing, for the Mn dimer structure, the exchange coupling is the dominant interaction, being two orders of magnitude larger than the DM interaction. In this same line of thought, in the next section we consider only the Heisenberg exchange and DM interactions to describe the magnetic properties of Mn trimers on the GaN(000$\bar{1}$) surface.

B. Trimers of Mn atoms on the GaN(000$\bar{1}$) substrate

Before explaining the magnetic interactions for the Mn trimers case, we describe the main structural features of the GaN(000$\bar{1}$) surface reconstruction we focus on in this paper. Through molecular beam epitaxy techniques followed by an annealing process, a submonolayer Mn deposition on the wurtzite GaN(000$\bar{1}$) 1×1 surface results in two unique surface reconstructions, depending on the substrate temperature [33]. At very low deposition temperature (less than 378 K), a $3a \times 3a$ structure is formed, whereas at higher deposition temperatures or after mild annealing of the $3a \times 3a$ reconstruction, a more stable $\sqrt{3}a \times \sqrt{3}a$-R30° structure forms [18]. The lowest energy structural model for the $3a \times 3a$ reconstruction is composed of trimers of Mn adatoms on the GaN(000$\bar{1}$) 1×1 surface [18]. Within the trimers, the Mn atoms are arranged in a triangular geometry and are located at H3 sites, as shown in the models seen in Fig. 7(a) top view and 7(b) side view. The Mn trimer is then slightly lifted up above, but centered at, the expanded equilateral triangle formed by three surface Ga atoms (which we label as Ga_s atoms, red in the figure). In turn, there is no Ga_s atom in the middle of the triangular close-packed Mn trimers. These Mn trimers have been observed in STM images of the $3a \times 3a$ reconstruction revealing regular arrays of triangular-shaped atomic protrusions as shown in Figs. 7(c), 7(d) and 7(e). Figure 7(c) shows the $3a \times 3a$ trimer lattice acquired at $V_s = -1.03$ V, $I_t = 47$ pA in which the individual trimers are seen as approximately spherical ball shapes with the individual atoms making up the trimers not being resolved. On the other hand, the clear details of the trimers are imaged at a slightly more negative sample bias as presented in Fig. 7(d), which was acquired at $V_s = -1.21$ V, $I_t = 63$ pA. In this image, it

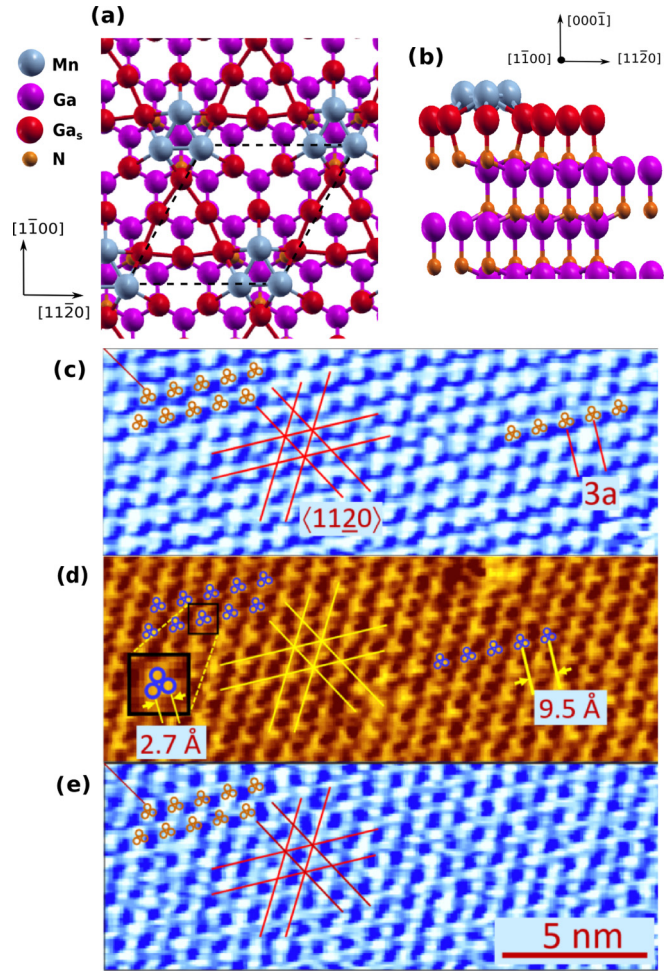

FIG. 7. Top panel: (a) Top and (b) side views corresponding to the lowest energy structural model for Mn trimers on top of the GaN(000$\bar{1}$) substrate. The color coding for each atom is stated in the legend. Ga_s stands for the Ga atom at the surface. Bottom panel: (c) High resolution STM image (in derivative mode) revealing a round ball-shaped protrusion at each trimer $3a \times 3a$ lattice site ($V_s = -1.03$ V, $I_t = 47$ pA); several envisioned trimer units are overlaid on top of the image; (d) higher resolution STM image (in derivative mode) of the $3a \times 3a$ trimer lattice acquired at $V_s = -1.21$ V, $I_t = 63$ pA; (e) dI/dV image (in derivative mode) acquired simultaneously with (c) at bias voltage $V_s = -1.03$ V.

is seen that each trimer lattice site corresponds to a triplet of atomic protrusions. The triplets are oriented such that a line drawn through the centers of any pair of trimer atoms within a trimer lies along one of the GaN ⟨11$\bar{2}$0⟩ high symmetry directions. Measurement of the atom-atom spacing within a trimer gives 2.7 Å ± 0.5 Å. The relatively large uncertainty reflects the difficulty of pinpointing the exact positions of the atoms within the trimers.

The dI/dV conductance image presented in Fig. 7(e) reveals a uniform 3×3 periodicity matching the constant current (CC) image (c) with the same lattice spacing $3a$. Although not showing clear intratrimer atomic resolution, the dI/dV image maxima (light blue) in (e) coincide with the locations of the trimers seen in the CC image (c), while the dI/dV minima (dark blue) correspond to regions in between

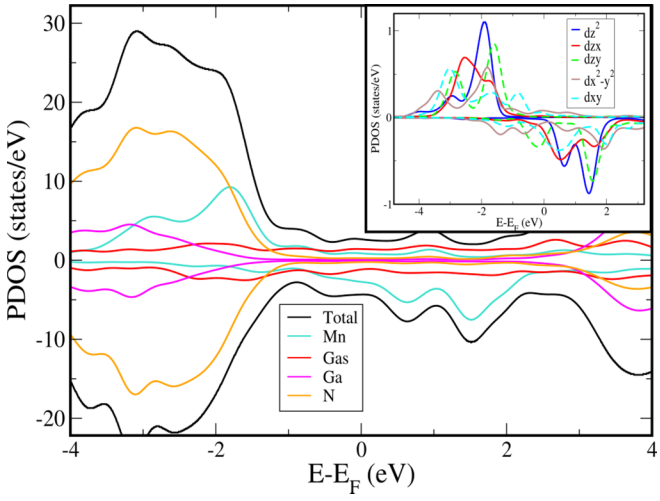

FIG. 8. Total density of states and projected density of states (PDOS) for the trimer of Mn adatoms on the GaN(000$\bar{1}$) substrate. The major contribution of the electronic states close to the Fermi level corresponds to the Ga$_s$ atomic levels. The Mn d orbitals are shown in the inset.

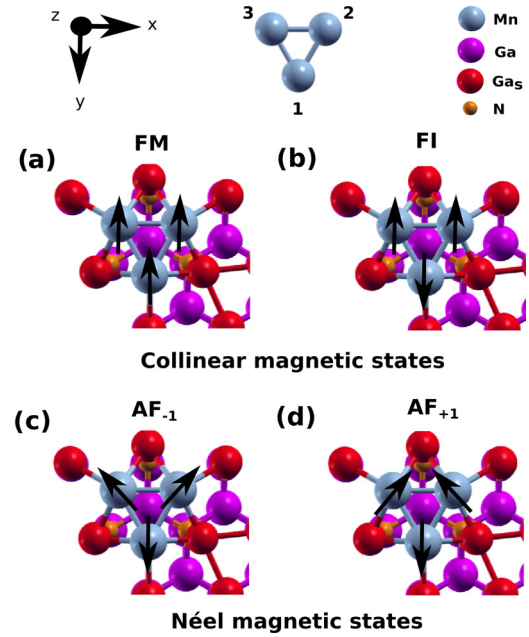

FIG. 9. Different magnetic configurations for a $3a \times 3a$-trimer Mn on the GaN(000$\bar{1}$) surface. (a) and (b) correspond to collinear magnetic states. (c) and (d) are the two lowest energy noncollinear magnetic configurations. The ground state corresponds to AF$_{-1}$.

the trimers. This indicates that the local density of states (LDOS) at $V_S = -1.03$ V is maximal at the trimers, in good agreement with the Tersoff-Hamman STM image simulation for occupied states shown in Ref. [18].

It is important to note that the 3×3 reconstruction experiences a structural transition upon annealing, towards the $\sqrt{3}a \times \sqrt{3}a$ reconstruction, which has long-range ferromagnetic ordering [19]. In the calculations, we have found that the magnetic ground state for the 3×3 structure is nonferromagnetic and therefore, it is expected that a magnetic transition, superimposed on the structural one, should occur upon annealing from the nonferromagnetic 3×3 surface reconstruction towards the ferromagnetic $\sqrt{3}a \times \sqrt{3}a$ one.

Figure 8 shows the PDOS for the Mn trimers on the GaN(000$\bar{1}$) substrate. In comparison with both the monomer and dimer Mn nanostructures, the presence of three Mn adatoms forming a trimer on the substrate has a major impact, noticeably on the electronic states at the Fermi level. In this case, both the Mn adatom d states and the Ga$_s$ levels have a major contribution at the Fermi level. The nondegeneracy of the Mn adatom d orbitals is evident in the inset of Fig. 8.

We now focus our attention on the magnetic properties of the triangular-shaped Mn trimers on the GaN(000$\bar{1}$) substrate, experimentally reported in Ref. [18] and shown in Fig. 7. To evaluate the magnetic ordering for the Mn atoms within the trimers, we took a lateral $3a \times 3a$ unit cell with the slab geometry described in Appendix A. The Mn adatoms are initially located at three H3 sites forming an equilateral triangle in which the Mn-Mn distances are 3.19 Å. In the first place, we performed spin-polarized *ab initio* calculations considering collinear spins for the Mn atoms of the trimers, proposing two magnetic configurations: a ferromagnetic one (FM) shown in Fig. 9(a) and a ferrimagnetic one (FI) which has one of the Mn spins of the trimer flipped with respect to the other two spins, as in Fig. 9(b). After relaxing the atomic structure, the FI configuration is the more stable one, being 5 meV/Mn lower in energy than the FM one. From the structural viewpoint, it is worth noticing that when the interaction between pairs of Mn atoms is ferromagnetic, the Mn-Mn distance relaxes towards the same value (2.63 Å). Similarly, when the pair interaction is antiferromagnetic, the Mn-Mn distance also has the same value but smaller than the ferromagnetically aligned case, namely 2.48 Å (see Table II). Thus, in the FM configuration the structure relaxes to an equilateral triangle of Mn adatoms, while for the FI configuration the structural relaxation renders an isosceles triangle. In both cases, as a result of atomic

TABLE II. Collinear and noncollinear magnetic states corresponding to the magnetic configurations depicted in Fig. 9. The relative energies per Mn (ΔE/Mn) and the magnitude of the magnetic moments for each Mn of the trimer μ_{Mn} are stated. For each magnetic configuration, the Mn-Mn distances ($d_{\mathrm{Mn}_i\text{-}\mathrm{Mn}_j}$) per pair of Mn atoms are shown (the numbers of the corresponding Mn atoms are indicated in parentheses and come from Fig. 9).

Magnetic state	ΔE/Mn (meV)	$d_{\mathrm{Mn}_i\text{-}\mathrm{Mn}_j}$ (Å)	μ_{Mn} (μ_{B})
FM	29	2.63	4.02
		2.63	4.02
		2.63	4.02
FI	24	2.63 (2-3)	3.88 (1)
		2.48 (1-2)	3.91 (2)
		2.48 (1-3)	3.91 (3)
AF$_{-1}$	0	2.50	3.32
		2.50	3.32
		2.50	3.32
AF$_{+1}$	0.030	2.50	3.32
		2.50	3.32
		2.50	3.32

relaxation, the Mn adatoms get closer compared to the initial distance. This structural behavior goes in the same line as the clustering tendency of Mn atoms within GaN reported in bulk [29].

At this point, it is important to remember that in the Mn dimer case, the nearest neighbor magnetic exchange interaction is antiferromagnetic. Hence, for the triangular-shaped Mn trimer on a hexagonal surface, such as GaN(000$\bar{1}$), the antiferromagnetic coupling between the Mn adatoms would lead to magnetic frustration due to the competition between the two antiferromagnetic interactions affecting each Mn spin in the trimer. Therefore, a noncollinear magnetic order is expected. On the basis of these results, noncollinear in-plane configurations are included hereafter to determinate the magnetic ground state of Mn trimers on top of GaN(000$\bar{1}$).

Following the formalism of Antal *et al.* [34] and considering only isotropic exchange coupling, the frustration induced by the geometry of the trimer leads to a Néel-type ground state with eightfold degeneracy, in which adjacent spins are at a 120° angle. These states can be broadly separated into two groups. On one hand, a group of two magnetic configurations composed of the Néel state shown in Fig. 9(c) (which we name AF_{-1}) and another configuration obtained by reversing all spin directions in Fig. 9(c). On the other hand, the second group consists of six equivalent configurations generated via C_{3v} symmetry transformations and time reversal of the magnetic configuration depicted in Fig. 9(d), called AF_{+1}. It is worth mentioning that the two groups of magnetic configurations have opposite chirality and that this chiral degeneracy can be lifted by DM interactions [34].

Our SOC electronic structure calculations show that the most stable magnetic configuration corresponds to AF_{-1}, in which the Mn spins are in-plane with the GaN(000$\bar{1}$) surface. After atomic relaxation, the Mn-Mn distance ($d_{Mn\text{-}Mn}$) contracts to 2.50 Å (see Table II and also note that the experimental STM measurement shown in Fig. 7 is in good agreement with this value), the value of the magnetic moment of each Mn atom is 3.32 μ_B and the total spin moment of the trimer is zero. The AF_{+1} chiral configurations are 0.030 meV/Mn above the AF_{-1} ground state energy and has the same $d_{Mn\text{-}Mn}$ distance and identical Mn magnetic moments.

Taking into account the orientation of the magnetic moments in the ground state, the contribution of the anisotropic exchange will be different from zero if the z component of the DM vector, D_z, takes a nonzero value. To estimate D_z, we define the chirality vector of the system as [34]

$$\mathbf{k} = \frac{2}{3\sqrt{3}} \sum_{i \neq j} (\mathbf{S_i} \times \mathbf{S_j}), \tag{3}$$

where the summation runs over the three directions of the bonds connecting the Mn atoms of the trimer, namely 1-2, 2-3, and 3-1 (the numbers correspond to the Mn atom labels in Fig. 9). The two groups of magnetic states can be assigned to the z component of the chirality vector, i.e., $k_z = -1$ [Fig. 9(c)] and $k_z = +1$ [Fig. 9(d)]. In our case, as the magnetic moments are in-plane with the surface of the substrate, the contribution of the anisotropic exchange coupling can be

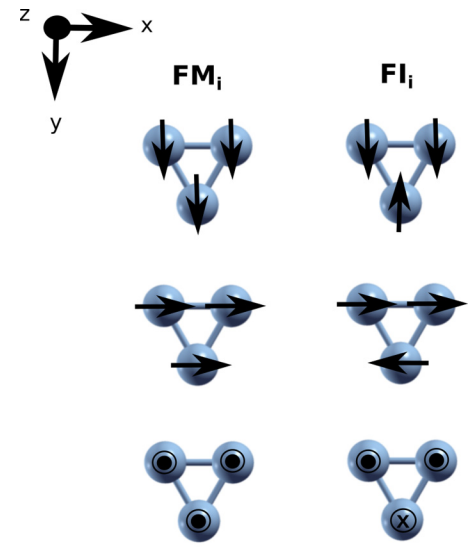

FIG. 10. Magnetic configurations considered to estimate the J values for the Mn trimers. The GaN substrate is omitted in the image to simplify the visualization of the magnetic configurations.

expressed as [34]

$$E_{\mathrm{DM}} = \frac{3\sqrt{3}}{2} D_z k_z. \tag{4}$$

Considering that the magnetic exchange interactions in both chiral structures are equivalent, we can estimate D_z from

$$D_z = \frac{\Delta E}{3\sqrt{3}S^2}, \tag{5}$$

where ΔE represents the energy difference between the chiral states labeled with $k_z = +1$ and $k_z = -1$. This estimation results in $D_z \sim 0.01$ meV.

The global symmetry of the trimer is C_{3v}. Each pair of Mn atoms presents a mirror plane bisecting the bond between them, and therefore the respective DM vector lies in this mirror plane, leading to one of the Moriya's rules. Thereby, the DM vectors have two components: an in-plane $D_\parallel$ and an out-of-plane D_z. The lines of the DM vectors cross each other at a common point lying on the C_{3v} symmetry axis of the Mn trimer. The three DM vectors of the system have, by symmetry, the same value for the D_z and $D_\parallel$ components. In this study, we only focus on the D_z components which distinguish between the two Néel states where the magnetic moments are in-plane with an angle of 120 degrees between each other.

To explore the magnetic exchange interactions J_i (for $i = x, y, z$) of the trimer, we take the crystal structure corresponding to the AF_{-1} ground state. The values of J_i can be estimated by taking the energy difference between FM (ferromagnetic) and FI (ferrimagnetic) configurations depicted in Fig. 10, corresponding to each coordinate axis, i.e., $J_i = \frac{\Delta E_i}{4S_i^2}$, where $\Delta E_i = E_{\mathrm{FM}_i} - E_{\mathrm{FI}_i}$.

Our results show that the values of J_i are all equal for each of the three axes ($J = 1.17$ meV). Thus, the isotropic nature of the exchange coupling interactions is revealed by the J_i values being equivalent for all the directions. Therefore, it

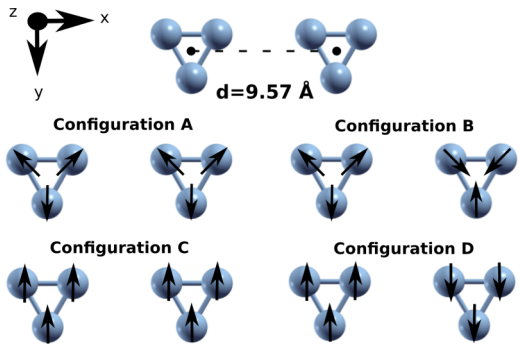

FIG. 11. Noncollinear magnetic configurations for two Mn trimers on top of the GaN(000$\bar{1}$) surface. The GaN substrate is omitted in the image to simplify the visualization of the magnetic configurations. The distance between trimers is 9.57 Å, as in the $3a \times 3a$ reconstruction reported in Ref. [18]. The ground state corresponds to configuration A.

can be concluded that the exchange coupling represents the predominant contribution to the magnetic interactions of the trimer, as it was also the case for the dimer structure.

Taking into account the energy scales of the involved interactions, we can conclude that the noncollinear magnetic order of the trimer is primarily due to the geometric frustration arising from exchange antiferromagnetic couplings. Another contribution comes from the DM interaction, which although being two orders of magnitude smaller than the isotropic exchange coupling is not negligible, and it is in fact responsible for the chiral degeneracy to be lifted.

C. Interaction between Mn trimers on the GaN(000$\bar{1}$) substrate

In this section we explore the magnetic interaction among Mn trimers on top of the GaN(000$\bar{1}$) substrate. We employ a lateral $6a \times 3a$ supercell (with the slab geometry described in Appendix A and place two Mn trimers at a distance of 9.57 Å as stated by the STM measurements (see Fig. 7 and Ref. [18]). We propose different magnetic configurations that are schematically depicted in Fig. 11. After performing atomic relaxation of this system, we found that the magnetic ground state has both trimers in the AF_{-1} arrangement as in configuration A. Table III states the energy differences with respect to the ground state, along with the total magnetic moment per cell for each configuration. The Mn trimers are sufficiently separated to prevent a strong overlapping of their electronic orbitals. Thus, there is no direct exchange interaction among them. Therefore, the energy difference between the A and B configurations (and similarly, between the C and D configurations) reveals the existence of indirect magnetic intertrimer interactions. These energy differences should be zero if the trimers were either isolated or supported on top of an inert substrate. The fact that those energy differences are roughly of the order of a few meV/Mn makes it plausible that the magnetic interaction among the trimers is mediated by the electronic states of the substrate, probably through its surface states.

TABLE III. Energy differences (ΔE) per Mn atom, for different magnetic configurations in the case of two Mn trimers on the GaN substrate, as depicted in Fig. 11. μ_{tot} is the magnetic moment of the cell for each case, and the magnitude of the magnetic moments for each Mn of the trimer μ_{Mn} are stated. In all cases the effect of atomic relaxation has been taken into account.

Configuration	ΔE/Mn (meV)	μ_{tot} (μ_B)	μ_{Mn} (μ_B)
A	0	0.00	3.35
B	1.8	0.00	3.35
C	29	23.60	3.60
D	27	0.00	3.60

Taking into account the presence of those surface GaN states (described in Sec. II), in the following we evaluate the role of the substrate in the magnetic interaction between pairs of Mn adatoms. We take a $9a \times 9a$ GaN(000$\bar{1}$) supercell with the same slab geometry previously considered. We evaluate the energy difference between the AF and FM configurations for each considered distance (d_{ij}) between the Mn adatoms. A schematic representation of a typical model structure for the calculations is shown in the top panel of Fig. 12 where for simplicity, only the first layers of the slab are shown. The Mn adatoms are located at H3 sites on the GaN(000$\bar{1}$) substrate, changing the distance between them for each calculation, describing a zigzag trajectory. For each given distance d_{ij}, we allow the local atomic relaxation of the Mn atoms as well as their nearest neighbor atoms, while the rest of the atoms in the cell are kept fixed. We then evaluate the energy difference between the FM and AF configurations (ΔE), but only at the Γ point due to the size of the supercell. This relation between ΔE and d_{ij} is plotted at the bottom panel of Fig. 12 (blue dots). As d_{ij} increases, the nature of the magnetic interaction changes, being antiferromagnetic for very short distances and thereafter having a damped oscillatory behavior between AFM and FM coupling. This type of indirect magnetic interaction in which the exchange coupling between the spin centers is mediated by the substrate electrons (surface states) is described by the Ruderman-Kittel-Kasuya-Yosida (RKKY) interaction [15–17].

The functional form describing the RKKY interaction in the asymptotic regime [35,36], originally derived for three-dimensional systems [15–17], is strongly dependent on the dimensionality and geometry of the system and is closely connected with the electronic structure of the host material. Indeed, the indirect interaction between adsorbates on a metal surface has its origin in the scattering of the substrate electrons at the adsorbed atoms, giving rise to electronic density oscillations (Friedel oscillations). The interference between such Friedel screening responses produces an oscillatory interaction between adsorbates [37,38]. When the substrate has a partially occupied surface state band, the interaction between adatoms on the surface decays as the inverse square of the separation between the adatoms [39,40] and oscillates with a period of half of the Fermi wavelength of the surface state band.

A nonperturbative description of the surface-state mediated adatom interaction has been developed by Hyldgaard and Persson [37]. In the asymptotic limit, the indirect adsorbate-adsorbate interaction ΔE, mediated by surface states, is given

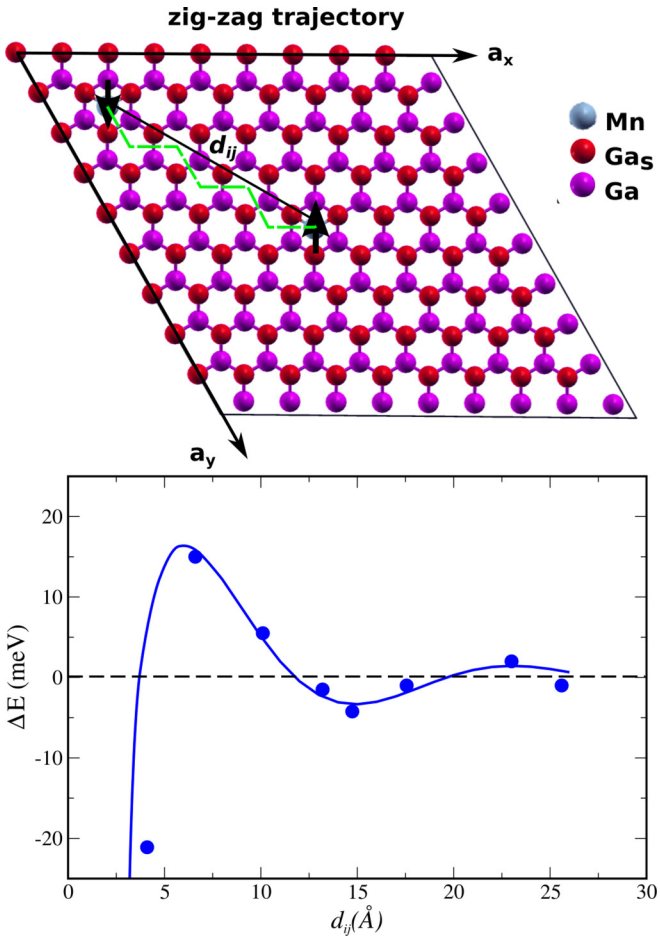

FIG. 12. Top panel: Top view of the supercell considered in the calculations. The two Mn adatoms are depicted with AF alignment and are located at H3 sites on top of the GaN(000$\bar{1}$) surface. Different calculations are carried out by progressively increasing the distance d_{ij} between the Mn adatoms, following a zigzag trajectory (green line). For each distance, both the FM and the AF spin configurations are calculated. Bottom panel: Energy difference between the AF and FM configurations, obtained with *ab initio* calculations, for different separations d_{ij} for the Mn adatom pair. The magnetic interaction presents a damped oscillatory behavior with d_{ij}. The smooth curving (blue) line is a fit to the calculated data points using Eq. (6).

by the analytical expression [37,38]:

$$\Delta E(d_{ij}) \simeq -\epsilon_F \left(\frac{2\sin(\delta_F)}{\pi}\right)^2 \frac{\sin(2q_F d_{ij} + 2\delta_F)}{(q_F d_{ij})^2}, \quad (6)$$

where d_{ij} is the distance between the two Mn adatoms, ϵ_F is the Fermi energy of the surface band (measured from the bottom of the band), q_F is the surface Fermi wave vector, and δ_F is the Fermi-level phase shift which describes the scattering properties of the adatom. The functional form described by Eq. (6) is derived considering an isotropic behavior of the surface state, in which q_F does not depend on the directionality of the interaction between the adatoms.

At this point it is important to emphasise that the RKKY interaction is mediated by conduction electrons close to the Fermi surface. This implies that on the GaN(000$\bar{1}$) surface, the interaction is dominated by the anisotropic B2 surface band with a d_{ij}^{-2} decay rate [41,42]. Despite the anisotropy of the surface state band, the smooth blue line depicted in Fig. 12 represents a surprisingly good fitting of our DFT results with the theoretical model described by Eq. (6). Table IV summarizes the main physical parameters extracted from the fit and also includes $\lambda_F/2$, which can be estimated as $\lambda_F/2 = \pi/q_F$.

TABLE IV. Main physical parameters extracted by the fitting of the DFT simulations results in the theoretical models described by Eq. (6).

ϵ_F (eV)	δ_F	q_F (Å^{-1})	$\lambda_F/2$ (Å)
0.73	0.42π	0.22	14

The bottom panel of Fig. 13 shows the dispersion relation of the B2 surface state band. The value of ϵ_F, measured from the bottom of the band, is in excellent agreement with the estimation from the fitting of Eq. (6). The q_F value should be interpreted in the context of the anisotropic behavior of the B2 band.

In Ref. [41], Patrone and Einstein derive an expression for the RKKY interaction mediated by anisotropic surface states. The wavelength of the oscillations is determined by the projection of the Fermi wave vector onto the direction of the vector connecting the two Mn adatoms, as discussed in detail in Refs. [41,42].

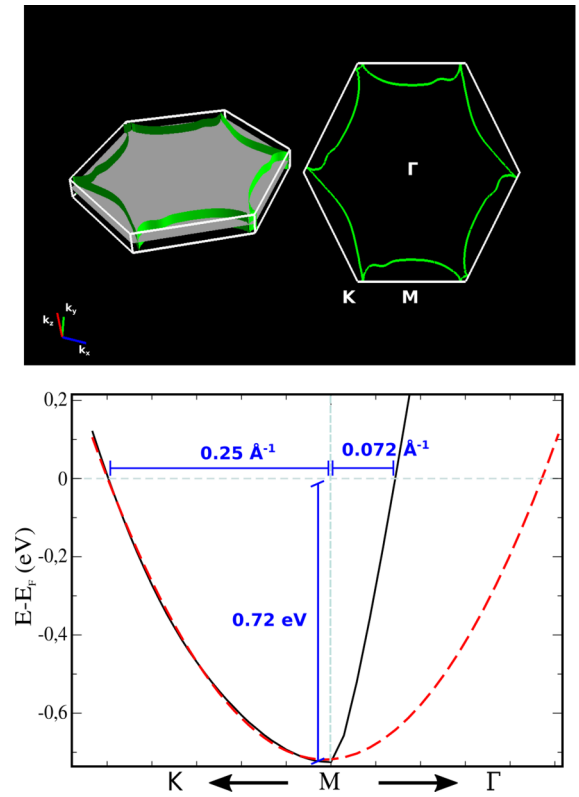

FIG. 13. Top panel: Fermi surface of the 1 × 1-GaN(000$\bar{1}$) substrate. Bottom panel: Fragment of B2 Fermi edge (black line) and free electronlike band state behavior, centered at the M point (dashed red line). The anisotropic character of B2 can be clearly evidenced comparing these two surface states.

Unlike the electronic states of certain noble metal surfaces, for example the Cu(111) surface in which an isotropic 2D electron gas behavior centered at the Γ point is present [43,44], in our case it is important to note the anisotropic nature of the GaN(000$\bar{1}$) B2 surface state that should imprint a direction-dependent asymptotic behavior to the RKKY interaction [41,42,45,46]. The anisotropic behavior of the B2 surface state can be clearly seen in the top panel of Fig. 13 where the Fermi surface of the 1×1-GaN(000$\bar{1}$) is plotted. The bottom panel of the same figure shows, for comparison, an hypothetical free electron band behavior centered at the M point (dashed red line) and the B2 surface state (black line). The degree of anisotropy in the B2 Fermi edge can be calculated from the comparison between the curvatures of the surface state band in two directions as shown in the bottom panel of Fig. 13. Hence, approximately 30% of anisotropic character can be attributed to the B2 surface state.

Since our data points in Fig. 12 (bottom panel) are calculated along different directions of the adatom pairs relative to the GaN(000$\bar{1}$) surface (as seen in the upper panel of the same figure), we might expect a variation of wavelengths. Therefore, it is difficult to relate the Fermi wave vector obtained from the isotropic model fit with the Fermi wave vectors corresponding to the surface state band. As a consequence, an isotropic model is not appropriate to describe the RKKY interaction between magnetic adatoms on the GaN(000$\bar{1}$) surface. To explore the directionality of the RKKY interaction in this surface a study must be performed involving the dependence of the magnitude of the adsorbate-adsorbate interaction over different directions on the GaN(000$\bar{1}$) surface in order to estimate each Fermi wave vector for every direction, but this approach is beyond the scope of the present paper.

To sum up, our results show that for small values of d_{ij}, the direct interaction among Mn spins dominates the magnetic interactions. As d_{ij} increases, the two-dimensional electron gas present at the GaN(000$\bar{1}$) surface mediates indirect magnetic interactions between Mn adatoms. Therefore, with our calculations we demonstrate the existence of an RKKY-type long-range exchange coupling between localized magnetic moments on a GaN(000$\bar{1}$) surface.

IV. CONCLUSIONS

In this work we perform noncollinear DFT calculations to elucidate the magnetic order of MnGaN 3×3 reconstructions with Mn triangular trimers. These reconstructions are formed by submonolayer Mn deposition on the N-polar face of wurtzite GaN(000$\bar{1}$). Using an effective spin Hamiltonian model, we explore and estimate the magnitude of the main interactions governing the magnetic state of this system. In the magnetic ground state configuration, the trimers are in a Néel state with the Mn spins being in-plane with the surface of the GaN(000$\bar{1}$) substrate. Our results show that the noncollinearity of the Mn magnetic moments in the trimers is driven by the geometric frustration of the exchange interaction and that the Dzyaloshinskii-Moriya interactions are essential for lifting the chiral degeneracy between the Néel states. Finally, we explore the nature and underlying mechanisms for the magnetic interaction between the Mn trimers and find that the substrate surface states play a key role, involving an RKKY-type interaction. These findings concerning the electronic and magnetic behavior of Mn adatoms on GaN(000$\bar{1}$) substrates open the path towards the development of nanoscale devices based on the transfer of spin information among magnetic clusters occurring through gallium nitride surface states.

ACKNOWLEDGMENTS

D.H, M.A.B, and V.F. would like to acknowledge support from CONICET (PIP0038) and ANPCyT (PICT1857). The authors thank the allocation of computational time in the HPC Cluster at CNEA. D.H. acknowledges CONICET for a postdoctoral fellowship. Experiments supported by the U.S. Department of Energy, Office of Basic Energy Sciences, Division of Materials Sciences and Engineering under Award No. DE-FG02-06ER46317.

APPENDIX: COMPUTATIONAL DFT METHODOLOGY

We use density functional theory (DFT) as implemented in the QUANTUM ESPRESSO code [47], which employs plane-wave basis functions and pseudopotentials to represent ion-electron interactions. Norm conserving type pseudopotentials are adopted, in combination with the LDA formalism for spin polarized calculations (LSDA), to compute the exchange-correlation term [48]. Our previous works show that the LDA exchange-correlation functional has been very accurate to reproduce the main electronic and structural properties of Mn nanostructures on GaN(000$\bar{1}$) surfaces [18,19,49]. Noncollinear calculations including spin-orbit coupling [50] are performed to assess the orientation of the magnetic moment into the trimer structure. The simulations are carried out for GaN slab supercells [GaN(000$\bar{1}$), $a = 3.19$ Å] with 11 layers, alternating Ga and N layers, and a vacuum of 15 Å is inserted between periodically repeated slabs. Pseudo-H atoms are added at the bottom layer of the slab in order to saturate the Ga dangling bonds [51]. The six topmost layers of the slab are relaxed while the other atoms of the structure are kept fixed to the positions corresponding to the GaN bulk crystal. The sampling of the Brillouin zone is done with a Monkhorst-Pack grid checking for convergence with the number of k points. To improve the numerical convergence, a first-order Methfessel-Paxton spreading is implemented [52] and a 0.005 Ry value for the Gaussian spreading for Brillouin-zone integration. All converged total energies are extrapolated to zero smearing. Energy cutoffs of 50 Ry and 400 Ry are used to expand the wave functions and the charge density, respectively. A $6 \times 6 \times 1$ k point is employed in the cases of supercells with either one, two, or three Mn adatoms on the GaN(000$\bar{1}$) surface. A $3 \times 6 \times 1$ k-point mesh is employed in the cases of two Mn trimers on the GaN(000$\bar{1}$) surface. An energy threshold of 10^{-6} Ry is used as a convergence criteria for geometry optimization. A threshold of 10^{-3} Ry/Bohr is considered for the forces. A posterior energy threshold of 10^{-8} Ry is used as a convergence criteria for self-consistence calculation of the optimized structures. The pseudopotentials are built using the scalar-relativistic Troullier-Martins scheme [53]. For the Mn atoms the $3s^2$ and $3p^6$ states are explicitly included in the calculations and the core radii are 1.7, 1.9, and 1.6 Bohr for the s,

p, and *d* states. For the Ga atom, the 3*d* electrons are included in the core. The pseudopotential core radii for Ga are 2, 2.5, and 1.9 Bohr for the *s*, *p*, and *d* orbitals, respectively, and 1.3 Bohr for the *s* orbitals and 1.45 Bohr for the *p* orbitals of N atoms. Fermi surfaces in this paper are drawn by using the FermiSurfer program [54].

[1] L. Balents, Spin liquids in frustrated magnets, Nature (London) **464**, 199 (2010).

[2] J. Knolle and R. Moessner, A field guide to spin liquids, Annu. Rev. Condens. Matter Phys. **10**, 451 (2019).

[3] M. Hervé, B. Dupé, R. Lopes, M. Böttcher, M. Martins, T. Balashov, L. Gerhard, J. Sinova, and W. Wulfhekel, Stabilizing spin spirals and isolated skyrmions at low magnetic field exploiting vanishing magnetic anisotropy, Nat. Commun. **9**, 1015 (2018).

[4] A. Kovalev and S. Sandhoefner, Skyrmions and Antiskyrmions in Quasi-Two-Dimensional Magnets, Front. Phys. **6**, 98 (2018).

[5] H. Reichlova, T. Janda, J. Godinho, A. Markou, D. Kriegner, R. Schlitz, J. Zelezny, Z. Soban, M. Bejarano, H. Schultheiss, P. Nemec, T. Jungwirth, C. Felser, J. Wunderlich, and S. T. B. Goennenwein, Imaging and writing magnetic domains in the non-collinear antiferromagnet Mn_3Sn, Nat. Commun. **10**, 5459 (2019).

[6] A. S. Núñez, R. A. Duine, P. Haney, and A. H. MacDonald, Theory of spin torques and giant magnetoresistance in antiferromagnetic metals, Phys. Rev. B **73**, 214426 (2006).

[7] A. B. Shick, S. Khmelevskyi, O. N. Mryasov, J. Wunderlich, and T. Jungwirth, Spin-orbit coupling induced anisotropy effects in bimetallic antiferromagnets: A route towards antiferromagnetic spintronics, Phys. Rev. B **81**, 212409 (2010).

[8] E. V. Gomonay and V. M. Loktev, Spintronics of antiferromagnetic systems, Low Temp. Phys. **40**, 17 (2014).

[9] O. Gomonay, V. Baltz, A. Brataas, and Y. Tserkovnyak, Antiferromagnetic spin textures and dynamics, Nat. Phys. **14**, 213 (2018).

[10] A. Bergman, L. Nordström, A. B. Klautau, S. Frota-Pessôa, and O. Eriksson, Magnetic interactions of Mn clusters supported on Cu, Phys. Rev. B **73**, 174434 (2006).

[11] A. Bergman, L. Nordström, A. Burlamaqui Klautau, S. Frota-Pessôa, and O. Eriksson, Magnetic structures of small Fe, Mn, and Cr clusters supported on Cu(111): Noncollinear first-principles calculation, Phys. Rev. B **75**, 224425 (2007).

[12] R. Cardias, M. M. Bezerra-Neto, M. S. Ribeiro, A. Bergman, A. Szilva, O. Eriksson, and A. B. Klautau, Magnetic and electronic structure of Mn nanostructures on Ag(111) and Au(111), Phys. Rev. B **93**, 014438 (2016).

[13] S. Lounis, Non-collinear magnetism induced by frustration in transition-metal nanostructures deposited on surfaces, J. Phys.: Condens. Matter **26**, 273201 (2014).

[14] J. Hermenau, Ibañez-Azpiroz, C. Hübner, A. Sonntag, B. Baxevanis, K. T. Ton, M. Steinbrecher, A. A. Khajetoorians, M. dos Santos Dias, S. Blügel, R. Wiesendanger, S. Lounis, and J. Wiebe, A gateway towards non-collinear spin processing using three-atom magnets with strong substrate coupling, Nat. Commun. **8**, 642 (2017).

[15] M. A. Ruderman and C. Kittel, Indirect exchange coupling of nuclear magnetic moments by conduction electrons, Phys. Rev. **96**, 99 (1954).

[16] T. Kasuya, A Theory of metallic ferro- and antiferromagnetism on Zener's mode, Prog. Theor. Phys. **16**, 45 (1956).

[17] K. Yosida, Magnetic properties of Cu-Mn alloys, Phys. Rev. **106**, 893 (1957).

[18] A. V. Chinchore, K. Wang, M. Shi, A. O. Mandru, Y. Liu, M. Haider, A. R. Smith, V. Ferrari, M. A. Barral, and P. Ordejón, Manganese 3×3 and $\sqrt{3} \times \sqrt{3} - R30^\circ$ structures and structural phase transition on w-GaN$(000\bar{1})$ studied by scanning tunneling microscopy and first-principles theory, Phys. Rev. B **87**, 165426 (2013).

[19] Y. Ma, A. V. Chinchore, A. R. Smith, M. A. Barral, and V. Ferrari, A Two-dimensional manganese gallium nitride surface structure showing ferromagnetism at room temperature, Nano Lett. **18**, 158 (2018).

[20] A. R. Smith, R. M. Feenstra, D. W. Greve, J. Neugebauer, and J. E. Northrup, Reconstructions of the GaN$(000\bar{1})$ Surface, Phys. Rev. Lett. **79**, 3934 (1997).

[21] S. Logothetidis, J. Petalas, M. Cardona, and T. D. Moustakas, Optical properties and temperature dependence of the interband transitions of cubic and hexagonal GaN, Phys. Rev. B **50**, 18017 (1994).

[22] O. Arbouche, B. Belgoumène, B. Soudini, and M. Driz, First principles study of the relative stability and the electronic properties of GaN, Comput. Mater. Sci. **47**, 432 (2009).

[23] A. R. Smith, R. M. Feenstra, D. W. Greve, M. S. Shin, M. Skowronski, J. Neugebauer, and J. E. Northrup, Determination of wurtzite GaN lattice polarity based on surface reconstruction, Appl. Phys. Lett. **72**, 2114 (1998).

[24] S. M. Widstrand, K. O. Magnusson, L. S. O. Johansson, and M. Oshima, Angle-resolved photoemission from stoichiometric GaN$(000\bar{1})$-(1×1), Surf. Sci. **584**, 169 (2005).

[25] B. J. Kowalski, R. J. Iwanowski, J. Sadowski, J. Kanski, I. Grzegory, and S. Porowski, Surface states on GaN$(000\bar{1})(1 \times 1)$-an angle-resolved photoemission study, Surf. Sci. **507**, 186 (2002).

[26] Y.-C. Chao, C. B. Stagarescu, J. E. Downes, P. Ryan, K. E. Smith, D. Hanser, M. D. Bremser, and R. F. Davis, Observation of highly dispersive surface states on GaN$(000\bar{1})1 \times 1$, Phys. Rev. B **59**, R15586(R) (1999).

[27] D. Gatteschi, R. Sessoli, and J. Villain, *Molecular Nanomagnets* (Oxford University Press, 2006).

[28] B. Nonas, I. Cabria, R. Zeller, P. H. Dederichs, T. Huhne, and H. Ebert, Strongly Enhanced Orbital Moments and Anisotropies of Adatoms on the Ag(001) Surface, Phys. Rev. Lett. **86**, 2146 (2001).

[29] X. Y. Cui, B. Delley, A. J. Freeman, and C. Stampfl, Neutral and charged embedded clusters of Mn in doped GaN from first principles, Phys. Rev. B **76**, 045201 (2007).

[30] F. Muñoz, A. H. Romero, J. Mejía-López, and J. L. Morán-López, First-principles theoretical investigation of monoatomic and dimer Mn adsorption on noble metal (111) surfaces, Phys. Rev. B **85**, 115417 (2012).

[31] F. Muñoz, A. H. Romero, J. Mejía-López, and J. L. Morán-López, Monoatomic and dimer Mn adsorption on the Au(111) surface from first principles, Phys. Rev. B **83**, 205423 (2011).

[32] T. Moriya, Anisotropic superexchange interaction and weak ferromagnetism, Phys. Rev. **120**, 91 (1960).

[33] A. V. Chinchore, K. Wang, W. Lin, and A. R. Smith, Atomic layer structure of manganese atoms on wurtzite gallium nitride (000$\bar{1}$), Appl. Phys. Lett. **93**, 181908 (2008).

[34] A. Antal, B. Lazarovits, L. Udvardi, L. Szunyogh, B. Újfalussy, and P. Weinberger, First-principles calculations of spin interactions and the magnetic ground states of Cr trimers on Au(111), Phys. Rev. B **77**, 174429 (2008).

[35] B. Gumhalter and W. Brenig, Indirect interactions between adsorbates in contact with quasi-one-dimensional surface electronic chain states, Surf. Sci. **336**, 326 (2008).

[36] T. L. Einstein, in *Physical Structure of Solid Surfaces*, edited by W. N. Unertl (Elsevier, Amsterdam, 1996), Vol. 2.

[37] P. Hyldgaard and M. Persson, Long-ranged adsorbate-adsorbate interactions mediated by a surface-state band, J. Phys.: Condens. Matter **12**, L13 (2000).

[38] P. Hyldgaard and T. L. Einstein, Surface-state mediated three-adsorbate interaction: electronic nature and nanoscale consequences, Surf. Sci. **532**, 600 (2003).

[39] N. Knorr, H. Brune, M. Epple, A. Hirstein, M. A. Schneider, and K. Kern, Long-range adsorbate interactions mediated by a two-dimensional electron gas, Phys. Rev. B **65**, 115420 (2002).

[40] K. H. Lau and W. Kohn, Indirect long-range oscillatory interaction between adsorbed atoms, Surf. Sci. **75**, 69 (1978).

[41] P. N. Patrone and T. L. Einstein, Anisotropic surface-state-mediated RKKY interaction between adatoms, Phys. Rev. B **85**, 045429 (2012)

[42] L. M. Roth, H. J. Zeiger, and T. A. Kaplan, Generalization of the Ruderman-Kittel-Kasuya-Yosida interaction for nonspherical fermi surfaces, Phys. Rev. **149**, 519 (1966)

[43] A. Tamai, W. Meevasana, P. D. C. King, C. W. Nicholson, A. de la Torre, E. Rozbicki, and F. Baumberger, Spin-orbit splitting of the Shockley surface state on Cu(111), Phys. Rev. B **87**, 075113 (2013).

[44] Z. Nie, I. Turcu, Y. Li, X. Zhang, L. He, J. Tu, Z. Ni, H. Xu, Y. Chen, X. Ruan, F. Frassetto, P. Miotti, N. Fabris, L. Poletto, J. Wu, Q. Lu, C. Liu, T. Kampen, Y. Zhai, W. Liu, C. Cacho, X. Wang, F. Wang, Y. Shi, R. Zhang, and Y. Xu, Spin-ARPES EUV Beamline for Ultrafast Materials Research and Development, Appl. Sci. **9**, 370 (2019).

[45] M. Zare, F. Parhizgar, and R. Asgari, Strongly anisotropic RKKY interaction in monolayer black phosphorus, J. Magn. Magn. Mater. **456**, 307 (2018)

[46] Y. Zhu, Y. F. Pan, Z. Q. Yang, X. Y. Wei, J. Hu, Y. P. Feng, H. Zhang, and R. Q. Wu, Ruderman-Kittel-Kasuya-Yosida Mechanism for Magnetic Ordering of Sparse Fe Adatoms on Graphene, J. Phys. Chem. C **123**, 4441 (2019)

[47] P. Giannozzi, S. Baroni, N. Bonini, M. Calandra, R. Car, C. Cavazzoni, D. Ceresoli, G. L. Chiarotti, M. Cococcioni, I. Dabo, A. Dal Corso, S. de Gironcoli, S. Fabris, G. Fratesi, R. Gebauer, U. Gerstmann, C. Gougoussis, A. Kokalj, M. Lazzeri, L. Martin-Samos, N. Marzari, F. Mauri, R. Mazzarello, S. Paolini, A. Pasquarello, L. Paulatto, C. Sbraccia, S. Scandolo, G. Sclauzero, A. P. Seitsonen, A. Smogunov, P. Umari, and R. M. Wentzcovitch, QUANTUM ESPRESSO: a modular and open-source software project for quantum simulations of materials, J. Phys.: Condens. Matter **21**, 395502 (2009).

[48] J. P. Perdew and A. Zunger, Self-interaction correction to density-functional approximations for many-electron systems, Phys. Rev. B **23**, 5048 (1981).

[49] Y. Ma, D. Hunt, K. Meng, T. Erickson, F. Yang, M. A. Barral, V. Ferrari, and A. R. Smith, Local strain-dependent electronic structure and perpendicular magnetic anisotropy of a Mn-GaN 2D magnetic monolayer, Phys. Rev. Materials **4**, 064006 (2020).

[50] A. Dal Corso and A. Mosca Conte, Spin-orbit coupling with ultrasoft pseudopotentials: Application to Au and Pt, Phys. Rev. B **71**, 115106 (2005).

[51] H. A. H. AL-Brithen, R. Yang, M. B. Haider, C. Constantin, E. Lu, A. R. Smith, N. Sandler, and P. Ordejón, Scanning Tunneling Microscopy and Surface Simulation of Zinc-Blende GaN(001) Intrinsic 4× Reconstruction: Linear Gallium Tetramers? Phys. Rev. Lett. **95**, 146102 (2005).

[52] M. Methfessel and A. T. Paxton, High-precision sampling for Brillouin-zone integration in metals, Phys. Rev. B **40**, 3616 (1989).

[53] N. Troullier and J. L. Martins, Efficient pseudopotentials for plane-wave calculations, Phys. Rev. B **43**, 1993 (1991).

[54] M. Kawamura, FermiSurfer: Fermi-surface viewer providing multiple representation schemes, Comput. Phys. Commun. **239**, 197 (2019).